JOURNAL OF GEOPHYSICAL RESEARCH, VOL. 99, NO. D4, PAGES 8183–8195, APRIL 20, 1994

Chemistry of the 1991-1992 stratospheric winter: Three-dimensional model simulations

F. Lefèvre,[1,2] G. P. Brasseur,[2] I. Folkins,[2,3] A. K. Smith,[2] and P. Simon[1]

Abstract. A three-dimensional chemistry-transport model of the stratosphere is used to simulate the evolution of trace constituents during the 1991-1992 Arctic winter. It is shown that heterogeneous reactions on polar stratospheric clouds led in early January to almost complete activation of atmospheric chlorine inside the polar vortex, in remarkable coincidence with observations by the ER-2 aircraft (*Toohey et al.*, 1993) and the microwave limb sounder on the Upper Atmosphere Research Satellite (*Waters et al.*, 1993). Sulfate aerosols resulting from the eruption of Mount Pinatubo also produced a significant increase in chlorine monoxide (ClO) concentrations at middle and high latitudes. The net chemical destruction of ozone found in the vortex at the end of the simulation (25% at 50 hPa and 25 DU), although substantial, was limited by available sunlight and the short period during which stratospheric clouds occurred.

1. Introduction

The potential for major ozone destruction in the Arctic existed in January 1992, when data from the satellite-borne microwave limb sounder (MLS) revealed the presence of an extensive maximum of chlorine monoxide (ClO) characterized by mixing ratios exceeding 2000 parts per trillion by volume (pptv) in the lower stratosphere [*Waters et al.*, 1993]. These ClO levels represent nearly all of the available inorganic chlorine in the lower stratosphere and are the highest values ever reported in the Arctic, similar to or even higher than those encountered during the formation of the ozone hole in Antarctica. As suggested by laboratory work [*Molina et al.*, 1987; *Tolbert et al.*, 1988; *Mozurkewich and Calvert*, 1988], the heterogeneous conversion of relatively stable chlorine reservoirs on polar stratospheric cloud (PSC) particles and sulfate aerosols is believed to be responsible for the formation of these high abundances of ozone-depleting ClO. Due to the eruption of Mount Pinatubo in June 1991 the 1991-1992 winter was also characterized by a highly enhanced aerosol load, estimated to be at least 1 order of magnitude larger than during nonvolcanic periods [*Brasseur and Granier*, 1992]. Further evidence for the unusual character of the 1991- 1992 stratospheric winter was provided by the long period of low-ozone columns (reduced by 20-25% compared to the long-term January mean) observed both by satellite [*Naujokat et al.*, 1992] and ground-based instruments [*World Meteorological Organization* (WMO), 1992a] over northern Europe and the Atlantic Ocean.

To analyze these dramatic perturbations, a three-dimensional simulation of the 1991-1992 winter was performed. The REPROBUS (reactive processes ruling the ozone budget in the stratosphere) model was used to assess the role played by heterogeneous processes occurring both on PSC and aerosol particles and to investigate the possibility of considerable ozone destruction during this period. Starting November 25, 1991, about 1 week before the occurrence of the first significant PSC event [*Newman et al.*, 1993], the model integrations were carried out until February 1, 1992, four days after the last PSC event in the simulation. The days of December 14, January 11, January 20, and February 1 are selected here to reflect the early stage of chlorine activation, the fully processed state, and to quantify the integrated ozone depletion at the end of the cold winter period.

2. Model Description

REPROBUS is a three-dimensional chemistry transport model that extends from the ground up to 10 hPa, with a vertical resolution varying from less than 1 km near the tropopause level to 2.2 km in the upper part of the stratosphere. The horizontal resolution used for this study is 2° latitude by 2° longitude. The densities of 41 chemical species or families are computed with a time step of 10 min (Table 1). Among them, 26 species are explicitly transported: these include typically long-lived species in the lower stratosphere (such as N_2O or HCl,

[1]Météo-France, Centre National de Recherches Météorologiques, Toulouse, France.

[2]National Center for Atmospheric Research, Boulder, Colorado.

[3]Now at Department of Oceanography, Dalhousie University, Halifax, Nova Scotia, Canada.

Paper number 93JD03476.
0148-0227/94/93JD03476$5.00

Table 1. Species or Families Included in REPROBUS

Transported	Photochemical Equilibrium
O_x	$O(^1D)$
CH_4	$O(^3P)$
H_2O	O_3
NO_y	H
HNO_3	OH
N_2O_5	HO_2
HO_2NO_2	N
NO_x	NO
$ClONO_2$	NO_2
Cl_y	NO_3
HCl	Cl
ClO_x	ClO
HOCl	Br
Cl_2	BrO
$ClNO_2$	BrCl
OClO	
Cl_2O_2	
H_2O_2	
HBr	
$BrONO_2$	
HOBr	
BrO_x	
N_2O	
CO	
Aerosols	
PSC tracer	

REPROBUS, reactive processes ruling the ozone budget in the stratosphere. PSC, polar stratospheric cloud.

for example), but also more unstable constituents which have a rather long lifetime in darkness (e.g., OClO, or Cl_2O_2). The photochemical module includes 72 gas phase reactions, based on the compilation by *DeMore et al.* [1992] (Table 2). Photodissociation frequencies (Table 3) are calculated for each time step and for each grid point using a four-dimensional lookup table expressed as a function of altitude, solar zenith angle, ozone column, and albedo. Cross sections are taken from *DeMore et al.* [1992], except for HOCl and HNO_3, for which more recent measurements by *Burkholder* [1993] and *Burkholder et al.* [1993] are used, respectively.

Heterogeneous processes are taken into account using a relatively detailed scheme that describes the condensation, sedimentation, and evaporation of PSC material [*Chipperfield et al.*, 1993]. Polar stratospheric clouds are first predicted as a function of H_2O and HNO_3 local partial pressures, using the saturation vapor pressures given by *Hanson and Mauersberger* [1988] for type I PSC (i.e., composed of nitric acid trihydrate crystals) and by *Murray* [1967] for type II water-ice PSC. The excess of H_2O and HNO_3 is removed from the gas phase when saturation occurs and is used to compute the surface area concentration in the PSC region, assuming a radius of 1 and 10 μm for type I and type II particles, respectively. Heterogeneous reaction rates are calculated explicitly, as a function of the surface area available, mean molecular velocity, and the reaction probabilities compiled in *WMO* [1992b] (Table 4). Note that the model does distinguish between type I and type II PSCs, the reactions on the latter being faster due to higher reaction probabilities and larger surface area. Furthermore, the PSC scheme includes a sedimentation of the cloud material, with a mean speed of 15 m/day and 1.5 km/day consistent with the size of type I and type II particles, respectively. The fallout of PSC particles affects the vertical distribution of H_2O, HNO_3, and HCl. Condensed species are returned to the gas phase when clouds evaporate.

Zonally symmetric initial tracer fields were taken from the two-dimensional model described by *Brasseur et al.* [1990]. Chlorine species were scaled to reach a total chlorine loading of 3.6 parts per billion by volume (ppbv) above 30 km near the pole [*WMO*, 1992b]. Winds and temperatures analyzed every 6 hours on 31 levels by the European Centre for Medium-Range Weather Forecasts (ECMWF) were used during the simulation to drive the transport of the stratospheric species and to compute their loss and production rates, respectively. Chemical species are advected using a semi-Lagrangian transport code, using a Hermite cubic interpolant with cubic derivative estimates modified to satisfy monotonicity [*Williamson and Rasch*, 1989]. Species are transported with a time step of 1 hour, along a trajectory calculated every 20 min.

3. Early Chlorine Activation

The first phase of the 1991-1992 Arctic winter was characterized by a strong and well-developed stratospheric vortex and by temperatures slightly below average [*Naujokat et al.*, 1992], leading to the sporadic formation of small-scale type I PSCs during the first days of simulation. The distribution and spatial extent of air masses chemically processed by PSCs can be assessed using an idealized tracer that indicates the time the air parcels have spent inside stratospheric clouds [*Lefèvre et al.*, 1991]. On December 14 the air exposed to heterogeneous chemistry earlier in the simulation is clearly identified at 50 hPa by a mass of "PSC tracer" stretching from the east coast of Greenland and Spitsbergen (where a small-scale PSC is predicted to be present), over Russia at 50°-60°N, and ending near the pole where the longest processing times are found (~50 hours, Figure 1a).

In the presence of PSCs, the following heterogeneous reactions convert relatively stable chlorine reservoirs (HCl, $ClONO_2$) into more reactive species (Cl_2, $ClNO_2$, HOCl):

$$ClONO_{2,g} + HCl_s \longrightarrow Cl_{2,g} + HNO_{3,s} \quad (73)$$

$$HOCl_g + HCl_s \longrightarrow Cl_{2,g} + H_2O_s \quad (74)$$

$$N_2O_{5,g} + HCl_s \longrightarrow ClNO_{2,g} + HNO_{3,s} \quad (75)$$

Table 2. Gas Phase Reactions in REPROBUS

No.	Reaction	Rate
1	$O + O + M \longrightarrow O_2 + M$	$k_1 = 4.23\times 10^{-28}[M]T^{-2}$ *
2	$O + O_2 + M \longrightarrow O_3 + M$	$k_2 = 6.0\times 10^{-34}[M](300/T)^{2.3}$
3	$O + O_3 \longrightarrow O_2 + O_2$	$k_3 = 8.0\times 10^{-12}\exp(-2060/T)$
4	$O(^1D) + N_2 \longrightarrow O + N_2$	$k_4 = 1.8\times 10^{-11}\exp(110/T)$
5	$O(^1D) + O_2 \longrightarrow O + O_2$	$k_5 = 3.2\times 10^{-11}\exp(70/T)$
6	$O(^1D) + H_2O \longrightarrow OH + OH$	$k_6 = 2.2\times 10^{-10}$
7	$O(^1D) + CH_4 \longrightarrow OH + CH3$	$k_7 = 1.4\times 10^{-10}$
8	$O(^1D) + H_2 \longrightarrow OH + H$	$k_8 = 1.0\times 10^{-10}$
9	$H + HO_2 \longrightarrow OH + OH$	$k_9 = 7.3\times 10^{-11}$
10	$H + HO_2 \longrightarrow H_2 + O_2$	$k_{10} = 6.5\times 10^{-12}$
11	$H + HO_2 \longrightarrow H_2O + O$	$k_{11} = 1.6\times 10^{-12}$
12	$H + O_3 \longrightarrow OH + O_2$	$k_{12} = 1.4\times 10^{-10}\exp(-470/T)$
13	$OH + O \longrightarrow H + O_2$	$k_{13} = 2.2\times 10^{-11}\exp(120/T)$
14	$OH + O_3 \longrightarrow HO_2 + O_2$	$k_{14} = 1.6\times 10^{-12}\exp(-940/T)$
15	$HO_2 + O_3 \longrightarrow OH + 2\ O_2$	$k_{15} = 1.1\times 10^{-14}\exp(-500/T)$
16	$HO_2 + O \longrightarrow OH + O_2$	$k_{16} = 3.0\times 10^{-11}\exp(200/T)$
17	$OH + HO_2 \longrightarrow H_2O + O_2$	$k_{17} = 4.8\times 10^{-11}\exp(250/T)$
18	$OH + H_2 \longrightarrow H_2O + H$	$k_{18} = 5.5\times 10^{-12}\exp(-2000/T)$
19	$H_2 + O \longrightarrow H_2O + H$	$k_{19} = 8.8\times 10^{-12}\exp(-4200/T)$
20	$HO_2 + NO \longrightarrow NO_2 + OH$	$k_{20} = 3.7\times 10^{-12}\exp(250/T)$
21	$HO_2 + HO_2 \longrightarrow H_2O_2 + O_2$	$k_{21} = 2.3\times 10^{-13}\exp(600/T)$
22	$OH + H_2O_2 \longrightarrow H_2O + HO_2$	$k_{22} = 2.9\times 10^{-12}\exp(-160/T)$
23	$OH + CO \longrightarrow CO_2 + H$	$k_{23} = 1.5\times 10^{-13}(1. + 0.6\times P/1013)$
24	$H + O_2 + M \longrightarrow HO_2 + M$	$k_{24} = 5.7\times 10^{-32}[M](300/T)^{1.6}$ *
25	$N + NO \longrightarrow N_2 + O$	$k_{25} = 3.4\times 10^{-11}$
26	$N_2O + O(^1D) \longrightarrow N_2 + O_2$	$k_{26} = 4.9\times 10^{-11}$
27	$N_2O + O(^1D) \longrightarrow NO + NO$	$k_{27} = 6.7\times 10^{-11}$
28	$NO_2 + O \longrightarrow NO + O_2$	$k_{28} = 6.5\times 10^{-12}\exp(120/T)$
29	$NO_2 + O_3 \longrightarrow NO_3 + O_2$	$k_{29} = 1.2\times 10^{-13}\exp(-2450/T)$
30	$NO + O_3 \longrightarrow NO_2 + O_2$	$k_{30} = 2.0\times 10^{-12}\exp(-1400/T)$
31	$N + O_2 \longrightarrow NO + O$	$k_{31} = 1.5\times 10^{-11}\exp(-3600/T)$
32	$HNO_3 + OH \longrightarrow H_2O + NO_3$	$k_{32} = 7.2\times 10^{-15}\exp(785/T)$ *
33	$HO_2NO_2 + OH \longrightarrow$ products	$k_{33} = 1.3\times 10^{-12}\exp(380/T)$
34	$NO_2 + OH + M \longrightarrow HNO_3 + M$	$k_{34} = 2.6\times 10^{-30}[M](300/T)^{3.2}$ *
35	$NO_2 + NO_3 + M \longrightarrow N_2O_5 + M$	$k_{35} = 2.2\times 10^{-30}[M](300/T)^{3.9}$ *
36	$NO_2 + HO_2 + M \longrightarrow HO_2NO_2 + M$	$k_{36} = 1.8\times 10^{-31}[M](300/T)^{3\ 2}$ *
37	$HO_2NO_2 + M \longrightarrow HO_2 + NO_2 + M$	$k_{37} = k_{36}/2.1\times 10^{-27}[M]\exp(10900/T)$
38	$N_2O_5 + M \longrightarrow NO_2 + NO_3 + M$	$k_{38} = k_{35}/4.0\times 10^{-27}[M]\exp(10930/T)$
39	$CH_4 + OH \longrightarrow CH_3 + H_2O$	$k_{39} = 2.9\times 10^{-12}\exp(-1820/T)$
40	$Cl + O_3 \longrightarrow ClO + O_2$	$k_{40} = 2.9\times 10^{-11}\exp(-260/T)$
41	$ClO + O \longrightarrow Cl + O_2$	$k_{41} = 3.0\times 10^{-11}\exp(70/T)$
42	$ClO + NO \longrightarrow Cl + NO_2$	$k_{42} = 6.4\times 10^{-12}\exp(290/T)$
43	$ClO + OH \longrightarrow Cl + HO_2$	$k_{43} = 1.1\times 10^{-11}\exp(120/T)$
44	$Cl + CH_4 \longrightarrow HCl + CH_3$	$k_{44} = 1.1\times 10^{-11}\exp(-1400/T)$
45	$Cl + H_2 \longrightarrow HCl + H$	$k_{45} = 3.7\times 10^{-11}\exp(-2300/T)$
46	$Cl + HO_2 \longrightarrow HCl + O_2$	$k_{46} = 1.8\times 10^{-11}\exp(170/T)$
47	$HCl + OH \longrightarrow Cl + H_2O$	$k_{47} = 2.6\times 10^{-12}\exp(-350/T)$
48	$ClONO_2 + O \longrightarrow$ products	$k_{48} = 2.9\times 10^{-12}\exp(-800/T)$
49	$ClO + NO_2 + M \longrightarrow ClONO_2 + M$	$k_{49} = 1.8\times 10^{-31}[M](300/T)^{3.4}$ *
50	$ClO + ClO + M \longrightarrow Cl_2O_2 + M$	$k_{50} = 1.9\times 10^{-32}[M](300/T)^{3\ 9}$ *
51	$Cl_2O_2 + M \longrightarrow ClO + ClO + M$	$k_{51} = k_{50}/3.0\times 10^{-27}[M]\exp(8450/T)$
52	$ClO + HO_2 \longrightarrow HOCl + O_2$	$k_{52} = 4.8\times 10^{-13}\exp(700/T)$
53	$HOCl + OH \longrightarrow H_2O + ClO$	$k_{53} = 3.0\times 10^{-12}\exp(-500/T)$
54	$HOCl + O \longrightarrow OH + ClO$	$k_{54} = 1.0\times 10^{-11}\exp(-2200/T)$
55	$HOCl + Cl \longrightarrow OH + Cl_2$	$k_{55} = 1.0\times 10^{-11}\exp(-2200/T)$
56	$OClO + OH \longrightarrow HOCl + O_2$	$k_{56} = 4.5\times 10^{-13}\exp(800/T)$
57	$OClO + Cl \longrightarrow ClO + ClO$	$k_{57} = 3.4\times 10^{-11}\exp(160/T)$
58	$OClO + O \longrightarrow ClO + O_2$	$k_{58} = 2.5\times 10^{-12}\exp(-950/T)$
59	$OClO + NO \longrightarrow ClO + NO_2$	$k_{59} = 2.5\times 10^{-12}\exp(-600/T)$

Table 2. (continued)

No.	Reaction	Rate
60	$Cl + NO_2 + M \longrightarrow ClNO_2 + M$	$k_{60} = 1.8\times 10^{-31}[M](300/T)^{2.0}$ *
61	$HBr + OH \longrightarrow H_2O + Br$	$k_{61} = 1.1\times 10^{-11}$
62	$BrO + O \longrightarrow Br + O_2$	$k_{62} = 3.0\times 10^{-11}$
63	$Br + O_3 \longrightarrow BrO + O_2$	$k_{63} = 1.7\times 10^{-11}\exp(-800/T)$
64	$BrO + NO \longrightarrow Br + NO_2$	$k_{64} = 8.8\times 10^{-12}\exp(260/T)$
65	$Br + HO_2 \longrightarrow HBr + O_2$	$k_{65} = 1.5\times 10^{-11}\exp(-600/T)$
66	$BrO + HO_2 \longrightarrow HOBr + O_2$	$k_{66} = 6.2\times 10^{-12}\exp(500/T)$
67	$Br + OClO \longrightarrow BrO + ClO$	$k_{67} = 2.6\times 10^{-11}\exp(-1300/T)$
68	$BrO + ClO \longrightarrow OClO + Br$	$k_{68} = 6.7\times 10^{-12}$
69	$BrO + ClO \longrightarrow Br + Cl + O_2$	$k_{69} = 2.9\times 10^{-12}\exp(220/T)$
70	$BrO + ClO \longrightarrow BrCl + O_2$	$k_{70} = 5.8\times 10^{-13}\exp(170/T)$
71	$BrO + BrO \longrightarrow 2\,Br + O_2$	$k_{71} = 1.4\times 10^{-12}\exp(150/T)$
72	$BrO + NO_2 + M \longrightarrow BrONO_2 + M$	$k_{72} = 5.2\times 10^{-31}[M](300/T)^{3.0}$ *

T is the temperature (K), [M] is the atmospheric density (cm^{-3}), and P is the pressure expressed in hPa.
*Low pressure limit.

$$ClONO_{2,g} + H_2O_s \longrightarrow HOCl_g + HNO_{3,s} \quad (76)$$

$$N_2O_{5,g} + H_2O_s \longrightarrow 2\,HNO_{3,s} \quad (77)$$

where g indicates that the molecule is in the gas phase and s in solution. As the reaction probability for reaction (73) is 100 times higher than for reaction (75) on type I PSCs [*Hanson and Ravishankara*, 1991a] and HOCl is rapidly removed heterogeneously by reaction (74) [*Abbatt and Molina*, 1992], the early presence of PSCs in the model led to an accumulation of Cl_2 in the processed areas. Once released from the PSC surface, the Cl_2 molecules, if exposed to sunlight, are immediately photolyzed to form chlorine atoms, which react rapidly with ozone to form ClO:

$$Cl + O_3 \longrightarrow ClO + O_2 \quad (40)$$

The three-step process described above (chlorine activation on PSC surface, Cl_2 photolysis, reaction with ozone) explains the presence of the ClO maximum predicted December 14 over western Russia, which occurs in a region where cloud processing was relatively short compared to the area located near the pole, but where solar light is present simultaneously (Figure 1b). The peak mixing ratio is 916 pptv at 50 hPa. This ClO level agrees well with the MLS observations on December 14 [*Douglass et al.*, 1993], which show a large ClO signal (~ 1 ppbv) centered on the same region at local noon (i.e., four hours earlier than in Figure 1*b*). As suggested by Douglass et al., our simulation shows that the ClO maximum observed by MLS on that day results from PSC processing north of the polar night terminator, followed by meridional transport and subsequent Cl_2 photolysis.

Sulfate aerosols in the lower stratosphere, enhanced after the eruption of Mount Pinatubo, also offer sites for heterogeneous processes. Since the solubility of HCl in the aerosol is believed to be considerably less than in ice [*Hanson and Ravishankara*, 1991b], the only reactions believed to be of importance are

$$ClONO_{2,g} + H_2O_{aerosol} \longrightarrow HOCl_g + HNO_{3,s} \quad (79)$$

$$N_2O_{5,g} + H_2O_{aerosol} \longrightarrow 2\,HNO_{3,s} \quad (80)$$

The rates for reactions (79) and (80) are calculated in the model as a function of the surface area available, the mean molecular velocity, and a reaction probability determined in the laboratory; the probability for reaction (79) (ranging from 1×10^{-2} to 1×10^{-4}) is computed as a function of the H_2SO_4 content of the aerosol (M. A. Tolbert, personal communication 1991), whereas

Table 3. Photolytic Reactions in REPROBUS

No.	Reaction
1	$O_2 + h\nu \longrightarrow O + O$
2	$O_3 + h\nu \longrightarrow O + O_2$
3	$O_3 + h\nu \longrightarrow O(^1D) + O_2$
4	$N_2O + h\nu \longrightarrow N_2 + O(^1D)$
5	$CH_4 + h\nu \longrightarrow$ products
6	$NO_2 + h\nu \longrightarrow NO + O$
7	$HNO_3 + h\nu \longrightarrow NO_2 + OH$
8	$HOCl + h\nu \longrightarrow Cl + OH$
9	$HO_2NO_2 + h\nu \longrightarrow$ products
10	$ClONO_2 + h\nu \longrightarrow ClO + NO_2$
11	$N_2O_5 + h\nu \longrightarrow NO_3 + NO_2$
12	$H_2O_2 + h\nu \longrightarrow OH + OH$
13	$OClO + h\nu \longrightarrow O + ClO$
14	$Cl_2O_2 + h\nu \longrightarrow Cl + Cl + O_2$
15	$HCl + h\nu \longrightarrow H + Cl$
16	$Cl_2 + h\nu \longrightarrow Cl + Cl$
17	$CO_2 + h\nu \longrightarrow CO + O$
18	$H_2O + h\nu \longrightarrow H + OH$
19	$ClNO_2 + h\nu \longrightarrow Cl + NO_2$
20	$BrONO_2 + h\nu \longrightarrow Br + NO_2$
21	$BrCl + h\nu \longrightarrow Br + Cl$
22	$HOBr + h\nu \longrightarrow Br + OH$
23	$NO + h\nu \longrightarrow N + O$

Table 4. Probabilities for Heterogeneous Reactions on PSCs and Sulfate Aerosols in REPROBUS

No.	Reaction	Type I	Type II
73	$ClONO_{2,g} + HCl_s \longrightarrow Cl_{2,g} + HNO_{3,s}$	0.3	0.3
74	$HOCl_g + HCl_s \longrightarrow Cl_{2,g} + H_2O_s$	0.1	0.3
75	$N_2O_{5,g} + HCl_s \longrightarrow ClNO_{2,g} + HNO_{3,s}$	0.003	0.03
76	$ClONO_{2,g} + H_2O_s \longrightarrow HOCl_g + HNO_{3,s}$	0.006	0.3
77	$N_2O_{5,g} + H_2O_s \longrightarrow 2\ HNO_{3,s}$	0.0006	0.03
		Sulfate Aerosol	
79	$ClONO_{2,g} + H_2O \longrightarrow HOCl_g + HNO_{3,g}$	$f(\%H_2SO_4)$ *	
80	$N_2O_{5,g} + H_2O \longrightarrow 2\ HNO_{3,g}$	0.1	

The g indicates that the molecule is in the gas phase and s indicates a solid solution.
*See text.

the value for reaction (80) was assumed to be 0.1 [*Hanson and Ravishankara*, 1991b; *Fried et al.*, 1994]. The initial surface area distribution was assumed to reach a maximum of 30 μm^2 cm^{-3} over the equator at 25 km and to decrease at midlatitudes with typical values of 12-18 μm^2 cm^{-3} at 20 km (D. J. Hofmann and L. Thomason, personal communications, 1992, and *NASA* [1993]). Substantially smaller values (0-1 μm^2 cm^{-3}) were initially prescribed inside the vortex, which was already largely isolated from the rest of the atmosphere when the Pinatubo cloud reached high latitudes. This aerosol surface area was then transported by the model winds, which resulted in a progressive penetration of the volcanic aerosols into the vortex, also reported from in situ measurements [*Rosen et al.*, 1992]. As shown in Figure 1*b*, our model predicts ClO levels between 50 and 150 pptv in the sunlit atmosphere over the Atlantic Ocean, Europe, and Middle East, in contrast with the 10-20 pptv calculated in a simulation in which heterogeneous chemistry is ignored. From Figure 1*a* it is clear that these elevated ClO abundances are obtained outside PSC-processed areas, and are therefore a result of the aerosol-catalyzed conversion of N_2O_5 and $ClONO_2$. ClO is directly enhanced by the photolysis of the relatively large amounts of HOCl (25-50 pptv on December 14) produced in the coldest air masses surrounding the vortex, where the probability of reaction (79) is highest. In addition, as N_2O_5 is rapidly removed by reaction (80) from regions where high aerosol loadings are encountered, NO_x (sum of NO and NO_2) levels are re-

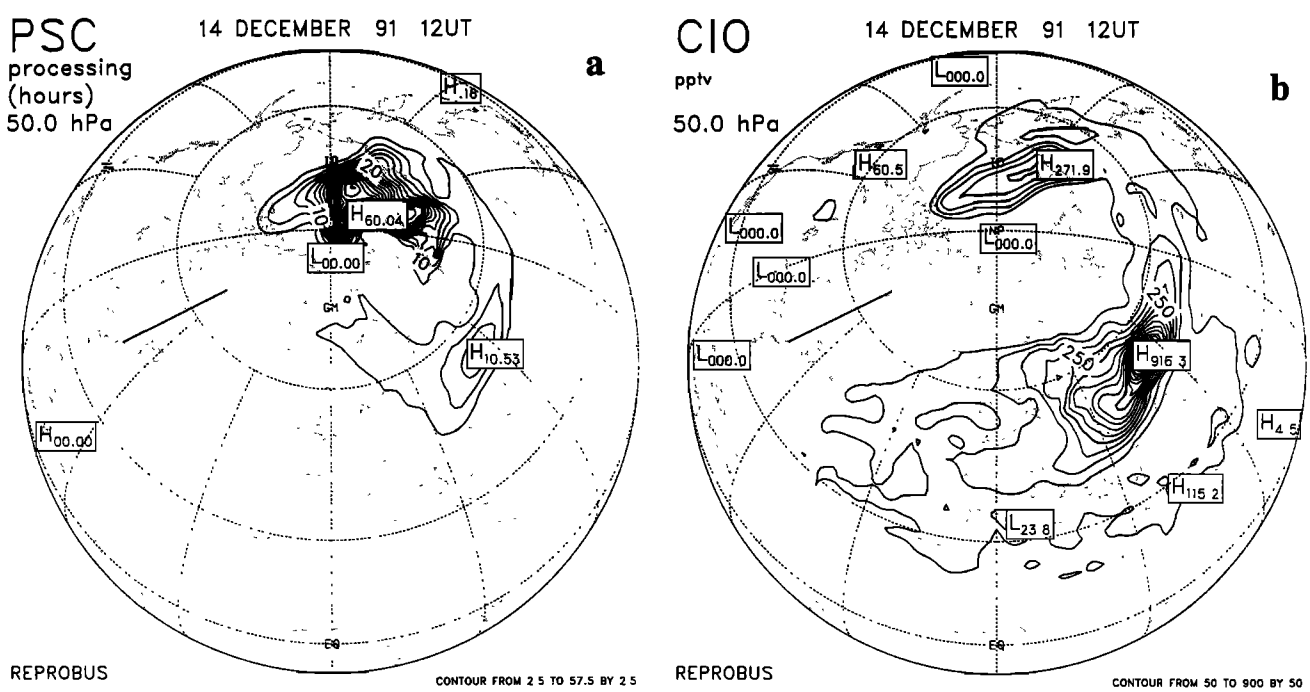

Figure 1. (a) Air processed by polar stratospheric clouds (PSCs; in hours spent inside PSCs) (b) ClO mixing ratio (pptv), and (c) NO_x mixing ratio (ppbv) calculated at 50 hPa on December 14, 1991, 1200 UT. The ER-2 flight path in the 60°- 70°W sector is also represented. Note the presence of PSCs near Spitsbergen (solid curve).

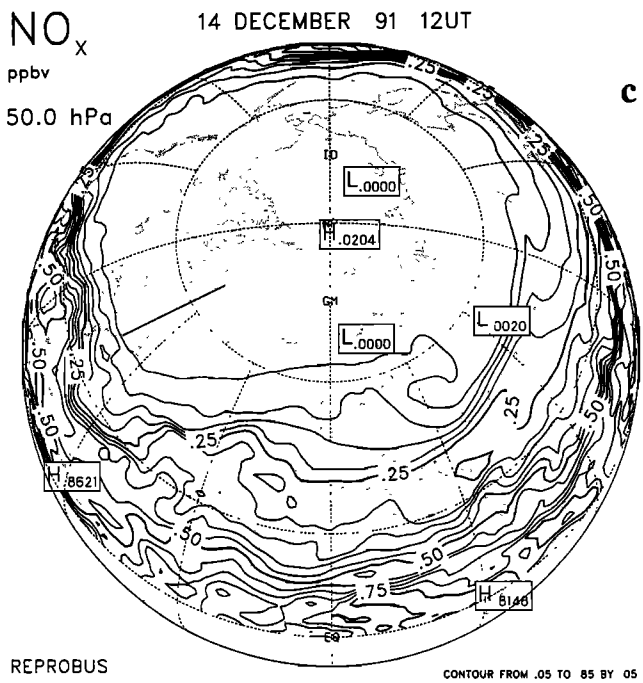

Figure 1. (continued)

duced by about 80% at mid-latitudes (Figure 1c). This process tends to inhibit the recombination of NO_2 and ClO to form $ClONO_2$.

The calculated ClO distribution is next compared to the measurements performed from the NASA ER-2 aircraft [*Toohey et al.*, 1993] which flew on December 14 from Bangor to a point located at 68°N, 61°W near Baffin Island. The ER-2 measured two profiles after the turning point and returned to Bangor along the same flight path. As suggested in Figure 1*a*, no PSC-processed air was encountered during the flight. During the morning (northbound) leg, ClO mixing ratios rose to approximately 30 pptv at 59°N before falling to less

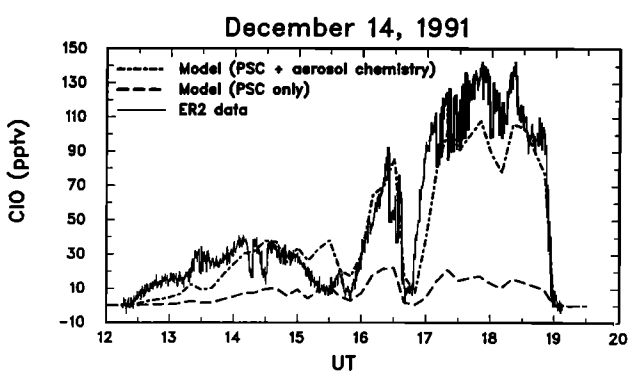

Figure 2. Comparison between observed ClO mixing ratios and model calculations interpolated along the ER-2 flight track on December 14, 1991. Results from two different simulations are shown. "PSC+aerosol chemistry" refers to a simulation in which heterogeneous chemistry on both PSCs and sulfate aerosol is taken into account. Sulfate aerosol chemistry is ignored in the "PSC only" case. ER-2 data are taken from *NASA* [1993].

than 10 pptv at the edge of the polar night (Figure 2). On the afternoon (southbound) leg, ClO increased rapidly (except during the dip performed by the aircraft between 1630 and 1700 UT), reaching values of 100-140 pptv before the final descent to Bangor. Model results were interpolated to coincide with the aircraft flight track. When heterogeneous processes occurring on sulfate aerosols are ignored, the modeled ClO abundance never exceeds 22 pptv, demonstrating that gas phase and PSC chemistries alone are unable to explain the high levels of observed ClO. When the conversions of N_2O_5 and $ClONO_2$ on aerosols are introduced, the model reproduces with much better agreement the slow ClO increase in the morning as well as the high levels (exceeding 100 pptv) and sharp variations encountered during the afternoon leg. These results, which are consistent with the ClO and NO_x levels predicted in Figure 1 (about six hours earlier), strongly suggest that the sulfate aerosol chemistry has significantly perturbed the chemistry of the lower stratosphere during the winter of 1991-1992. In these conditions it is also concluded that the peeling off of PSC-processed air from within the vortex is not necessary to reach the ClO amounts of ~100 pptv measured in midlatitudes from the ER-2; this conclusion holds on even if the model has underestimated the number of blobs of ex-vortex air because of insufficient horizontal resolution [see *Tuck et al.*, 1992].

4. Fully Processed State in January

The 1991-1992 Arctic winter included a period during which low temperatures allowed for the quasi-continuous presence of type I PSCs from December 24 until January 28. We focus here on the fields obtained from the model on January 11, during the period when the chlorine radicals reached their highest concentrations in the lower stratosphere. At 50 hPa, type I PSCs were thermodynamically possible over a large area extending from Spitsbergen to Denmark and from eastern Greenland to the Kola peninsula (Plate 1*a*; note that no type II PSCs were predicted during the simulation). These clouds were quasi-stationary and therefore able to process large volumes of stratospheric air over a few days. In contrast to the localized perturbation observed December 14, on January 11 the entire vortex had been exposed to heterogeneous chemistry (Plate 1a). Air masses located in the core of the vortex had spent between 150 and 250 hours inside the cloud regions, where the effects of heterogeneous reactions led primarily to a large accumulation of Cl_2 at the expense of HCl and $ClONO_2$. Plate 1*b* shows that Cl_2 reached 1300 pptv on January 11 and became the major form of chlorine in the polar air not exposed to sunlight. The sharp gradient predicted at the edge of the polar night reflects the fast photolysis of Cl_2, which occurs almost instantaneously in sunlit regions.

The strongest chemical perturbations, however, took place at the inner edge of the vortex, where significantly

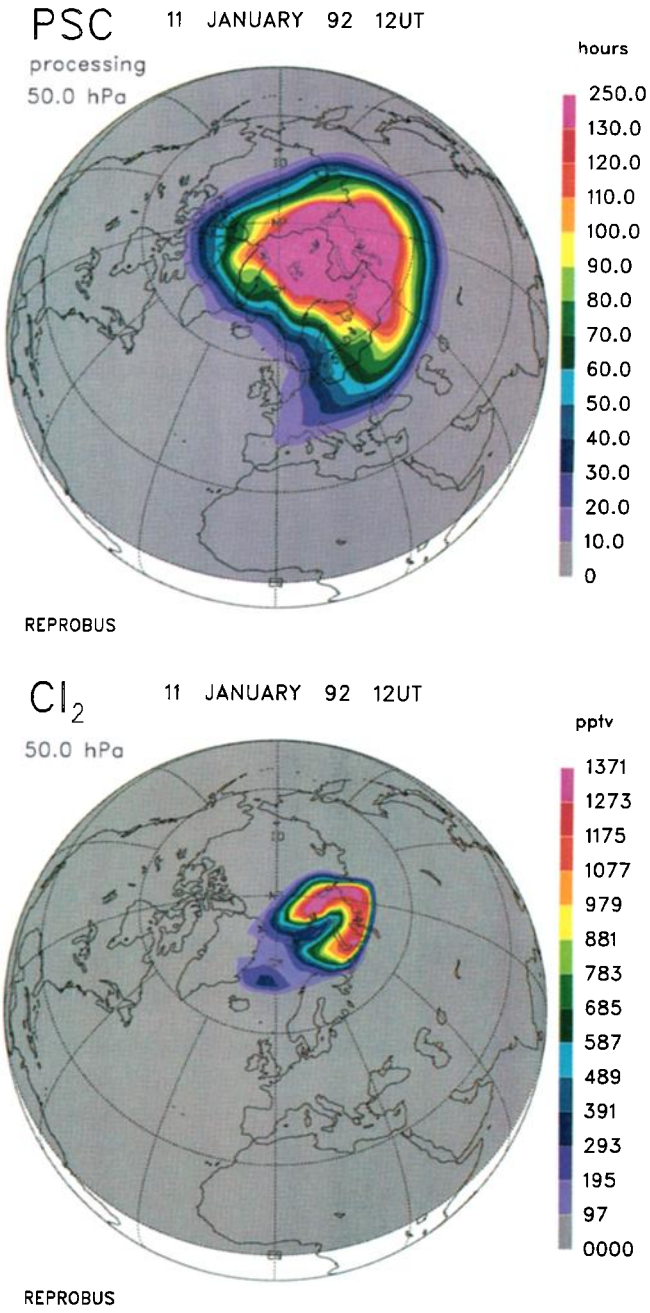

Plate 1. (a) Air processed by polar stratospheric clouds (in hours spent inside PSCs), and (b) Cl_2 mixing ratio (pptv) calculated at 50 hPa on January 11, 1992, 1200 UT. The black line indicates the area covered by PSCs on that day.

processed air was exposed to sunlight over western Europe and Russia. The enhanced PSC activity and subsequent Cl_2 decomposition in early January led to a dramatic rise in ClO, well simulated by the model. On January 11 the displacement of the vortex away from the pole allowed a large fraction of Cl_2-rich air to be exposed to sunlight, resulting in extremely high ClO levels produced by the model (1000-1800 pptv at 50 hPa) over Scandinavia and Russia, between the polar night terminator at 69°N and latitudes as low as 40°N.

For easy comparison with the MLS data, Plate 2 represents the ClO mixing ratio calculated on the 465 K isentrope surface for local noon at all locations. Although the diurnal variation is removed in the figure, significant longitudinal variations are seen within the vortex. The maximum ClO mixing ratios are found over western Russia, where the polar air is rapidly processed through the type I PSC, identified in Plate 1a, and Cl_2, $ClNO_2$ are rapidly photolyzed. The peak mixing ratio on the 465 K isentrope exceeds 1900 pptv. Such amounts are approximately 50% higher than the largest ClO values measured during the formation of the 1987 ozone hole in Antarctica and during February 1989 in the Arctic [*Brune et al.*, 1991]. The slightly lower ClO values found over western Europe are consistent with less PSC processing calculated over these regions in Plate 1a. Farther east, away from the PSC region and the ClO maximum at 50°E the decrease in ClO abundances reflects a partial deactivation of the chlorine radicals into more stable forms. Although less than 100 pptv of NO_x were initially available in the vortex, the titration of ClO by NO_2 to form $ClONO_2$ probably explains in part the eastward decrease of the ClO abundance. The calculated distribution of $ClONO_2$ inside the vortex (Plate 3*a*) shows mixing ratios that increase from 0.1 to 0.6 ppbv along the 60°N latitude circle, suggesting that a significant source of NO_x was present. A detailed analysis shows that the HNO_3 temperature-dependent photolysis rate was reduced during this period and that the reaction with OH provided the major

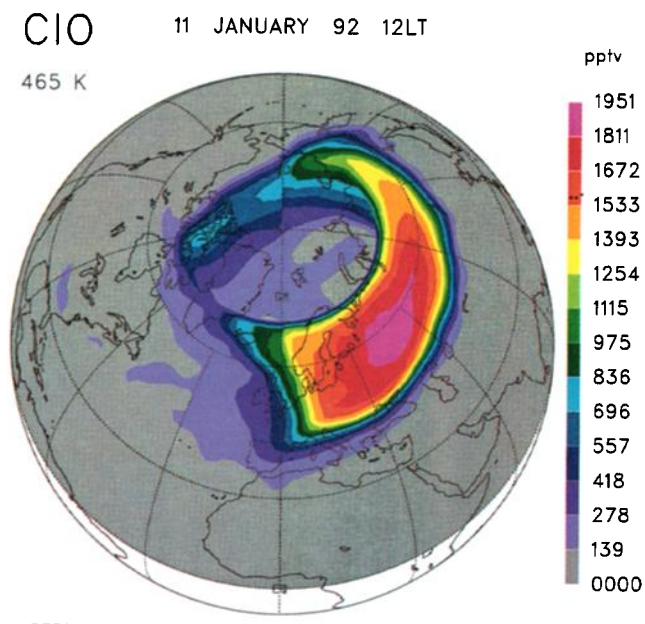

Plate 2. ClO distribution calculated on the 465 K isentrope surface on January 11, 1992. The field was mapped at all locations for local noon to achieve better temporal coincidence with satellite measurements (note the discontinuity on both sides of the dateline). See Figure 3 in the work of *Waters et al.* [1993] for a comparison with microwave limb sounder observations.

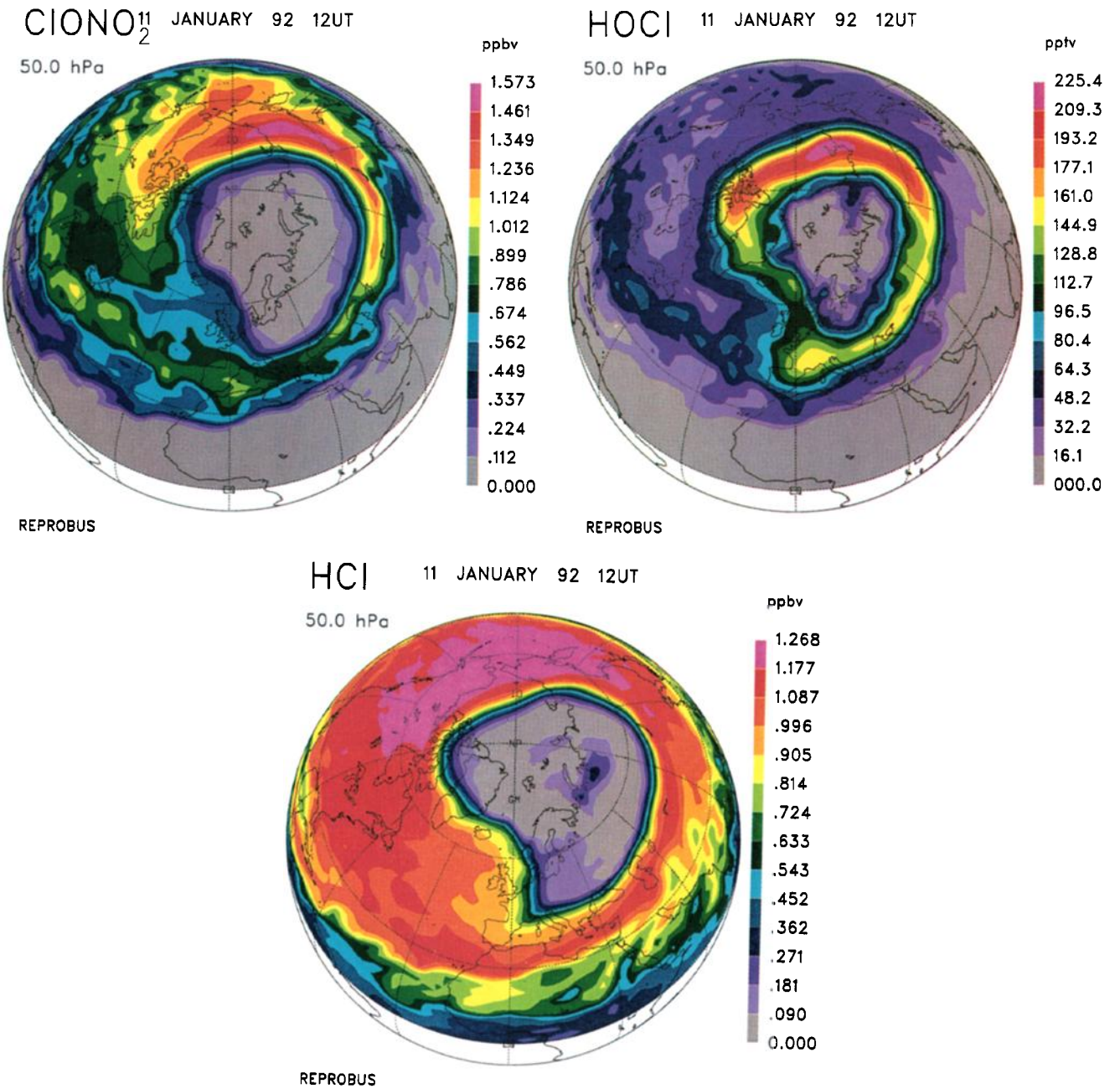

Plate 3. (a) $ClONO_2$ mixing ratio (ppbv), (b) HOCl mixing ratio (pptv), and (c) HCl mixing ratio (ppbv) calculated at 50 hPa on January 11, 1992, 1200 UT.

external source of NO_x:

$$HNO_3 + OH \longrightarrow H_2O + NO_3 \quad (32)$$

The ClO abundance along the airflow is also affected by the daytime reaction with HO_2 forming HOCl. This reaction is particularly efficient at low temperatures (time constant of 4 hours at 200 K) and leads to the formation of large HOCl concentrations in the polar air exposed to sunlight (Plate 3*b*). In January 1992, large amounts of HOCl were passively transported eastward through the polar night toward the Iceland-Spitsbergen region, where PSCs were present. As discussed by *Crutzen et al.* [1992], the simultaneous presence of high levels of HOCl, sunlight, and polar stratospheric clouds may lead to strongly enhanced conversion of HCl to ClO, via the following cycle :

$$ClO + HO_2 \longrightarrow HOCl + O_2 \quad (52)$$
$$HOCl_g + HCl_s \longrightarrow Cl_{2,g} + H_2O_s \quad (74)$$
$$Cl_2 + h\nu \longrightarrow 2\,Cl \quad (J_{16})$$
$$2(Cl + O_3 \longrightarrow ClO + O_2) \quad (40)$$
$$\text{net} : HCl + HO_2 + 2O_3 \longrightarrow ClO + H_2O + 3O_2$$

This cycle is potentially very important since a complete heterogeneous removal of HCl may be accomplished by reaction (74) which, unlike heterogeneous reaction (73), is not limited by the availability of $ClONO_2$.

The HCl distribution obtained on January 11 demonstrates the significance of this process. Plate 3c shows that HCl has been totally removed in the PSC-processed regions by the combined effects of reaction with $ClONO_2$ and the cycle described above. Thus it is shown that near-zero mixing ratios of HCl can be achieved despite the initial excess of HCl prescribed in the model (the ratio $HCl/ClONO_2$ was between 1.5 and 2 at 20 km). As HOCl is permanently regenerated by reaction (52) in daylight, the complete removal of HCl leads eventually to the buildup of a "collar" of HOCl at the inner edge of the vortex (Plate 3b), which also contributes to the calculated longitudinal variation of ClO.

The derived ClO fields may be compared with the MLS observations presented by *Waters et al.* [1993]. Their Figure 3 is directly comparable to the modeled ClO distribution mapped at local noon on January 11 and on the 465 K surface (Plate 2). The model reproduced remarkably well the geographical extent of the enhanced ClO area as well as the longitudinal variation observed from 50°E to eastern Siberia where the perturbed air entered the polar night. Interestingly, the model is also able to "complement" the MLS coverage beyond 80°N, where high ClO levels (~700 pptv) calculated on the warmer side of the vortex indicate that thermal equilibrium was established between ClO and

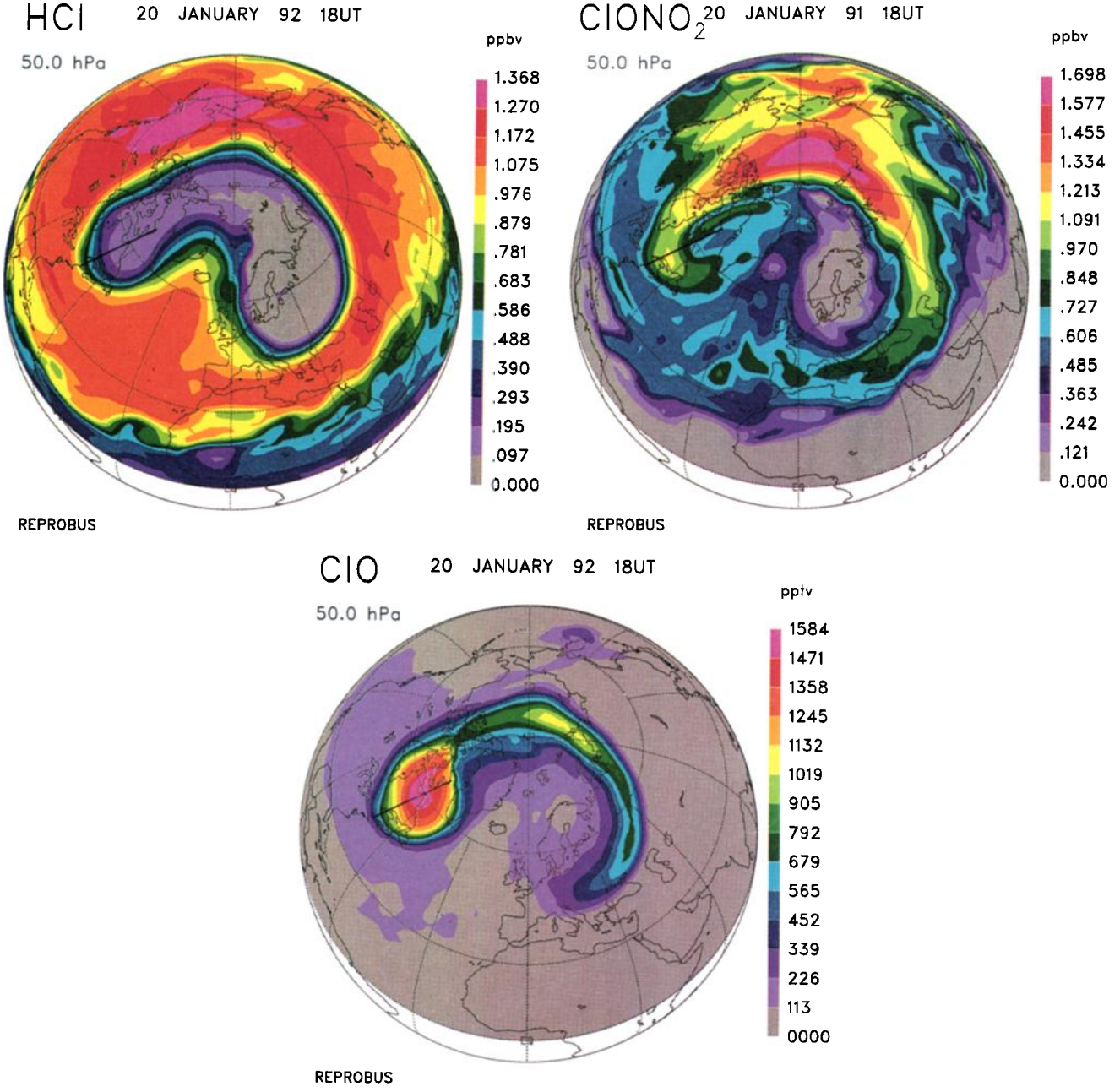

Plate 4. (a) HCl mixing ratio (ppbv), (b) $ClONO_2$ mixing ratio (ppbv), and (c) ClO mixing ratio (pptv) calculated at 50 hPa on January 20, 1992, 1800 UT. The ER-2 flight path in the 60°-70°W sector is also represented.

Cl_2O_2. The maximum ClO abundances produced by the model at 465 K are somewhat lower than those observed by MLS, which were often in excess of 2 ppbv over large areas in early January 1992. This discrepancy could be explained by the possible overestimation of the ClO retrieved from MLS in regions where nitric acid is removed from the gas phase (J. Waters, personal communication, 1993). Alternatively, the maximum ClO levels reported by Waters et al. may indicate that surprisingly high levels of total inorganic chlorine (Cl_y) were present in the Arctic lower stratosphere, exceeding by at least 10% the Cl_y abundance present in the model (2.6- 3.0 ppbv in the enhanced ClO area at 50 hPa), or that current photochemical data for the ClO-Cl_2O_2 equilibrium and Cl_2O_2 absorption cross sections lead to an overestimation in the model of the daytime Cl_2O_2 abundance (250 to 500 pptv depending on solar zenith angle) and therefore to an underestimation of ClO.

ClO levels in excess of 1.5 ppbv were also measured from the ER-2 aircraft during the January 20, 1992, flight [*Toohey et al.*, 1993], at a time when the vortex was distorted by a strong blocking anticyclone over Iceland. The vortex shape at 50 hPa is clearly defined by the sharp gradients of HCl calculated by the model (Plate 4*a*). It may be seen that the flight track entered the vortex very early in the flight and penetrated deep inside the chemically perturbed region. The modeled HCl mixing ratios along the flight track are between 0.1 and 0.2 ppbv, in good agreement with the values measured from the ER-2 by the ALIAS instrument [*Webster et al.*,1993]. Lower HCl mixing ratios (less than 0.1 ppbv) are predicted by the model over Europe, where extended PSCs were still present on January 20. Plate 4*b* plots the corresponding mixing ratios of $ClONO_2$, which show a large variability within the vortex. This reflects the relatively fast recovery of this gas that occurred in the air masses transported from Scandinavia, where PSCs are present, to the warmer region sampled by the ER-2 over North America. Thus because the recovery of HCl takes place on a much longer timescale, there is not a same relationship among HCl, $ClONO_2$, and reactive chlorine in both lobes of the vortex, and an excess of $ClONO_2$ is calculated by the model along the aircraft flight track. This is consistent with the analysis by Webster et al. that shows incomplete chlorine activation during the January 20 flight and significant departures from the 1:2 line predicted from the stoichiometry of reaction $HCl + ClONO_2 \rightarrow 2Cl + HNO_3$. The ClO distribution calculated by our model during the return leg of the ER-2 shows that the aircraft flew through the region where ClO was maximum at 1800 UT (Plate 4*c*). The modeled ClO interpolated along the flight track agrees well with the ER-2 data (Figure 3). Differences are of the order of 10%, except near the vortex edge at the end of the flight when the model cannot reproduce horizontal gradients as sharp as in the real atmosphere. The modeled BrO distribution (not shown) also shows relatively good agreement with the ER-2 measurements, with high levels between 8 and 11 pptv along the flight track.

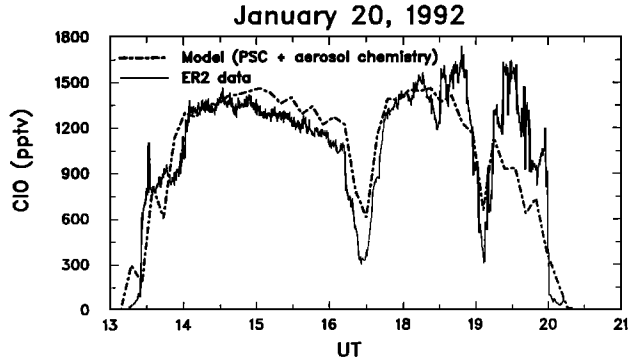

Figure 3. Comparison between observed ClO mixing ratios and model calculations interpolated along the ER-2 flight track on January 20, 1992. ER-2 data are taken from *NASA* [1993].

The ClO abundance in the rest of the vortex not exposed to sunlight (see Plate 4c) is lower and is directly controlled by the ClO/Cl_2O_2 thermal equilibrium, as shown by the relatively large values (~1 ppbv) obtained near the pole at 225-230 K, which contrast with the 50-100 pptv predicted above northern Scandinavia at 190-192 K. Interestingly, the model shows a region over Kamchatka with unusually high nighttime midlatitude ClO (200-300 pptv). Inspection of hourly model output reveals that this area coincides with a blob of polar air peeled off from the vortex, a fact that is confirmed by the high potential vorticity values observed in this region (see Figure 3a in the work of *Webster et al.*, [1993]) and by the localized HCl minimum indicating earlier PSC processing (Plate 4a). This result supports the mechanism suggested by *Tuck et al.* [1992], which shows that high ClO amounts may persist in blobs of air exported from the vortex and therefore contribute to midlatitude ozone loss. The January 20 event was however the only significant peel-off event simulated by the model at 50 hPa.

5. Ozone Depletion

The chemical perturbation simulated in January 1992 had the potential for considerable ozone destruction. During this period, ozone loss rates in excess of 4×10^6 molecules cm^{-3} s^{-1} were found at 20 km in the enhanced ClO and BrO area. These values are even higher than the destruction rates derived at this altitude during the formation of the 1987 Antarctic ozone hole [*Murphy*, 1991]. However, in contrast to the ~12 hours of sunlight per day available during the Antarctic spring, catalytic cycles operate for only ~5 hours/day at 61°N in early January. Furthermore, due to the nonzonal circulation observed during this period, the chemically perturbed air parcels spent one third to one half of their circumpolar trajectory in the polar night (see, for in-

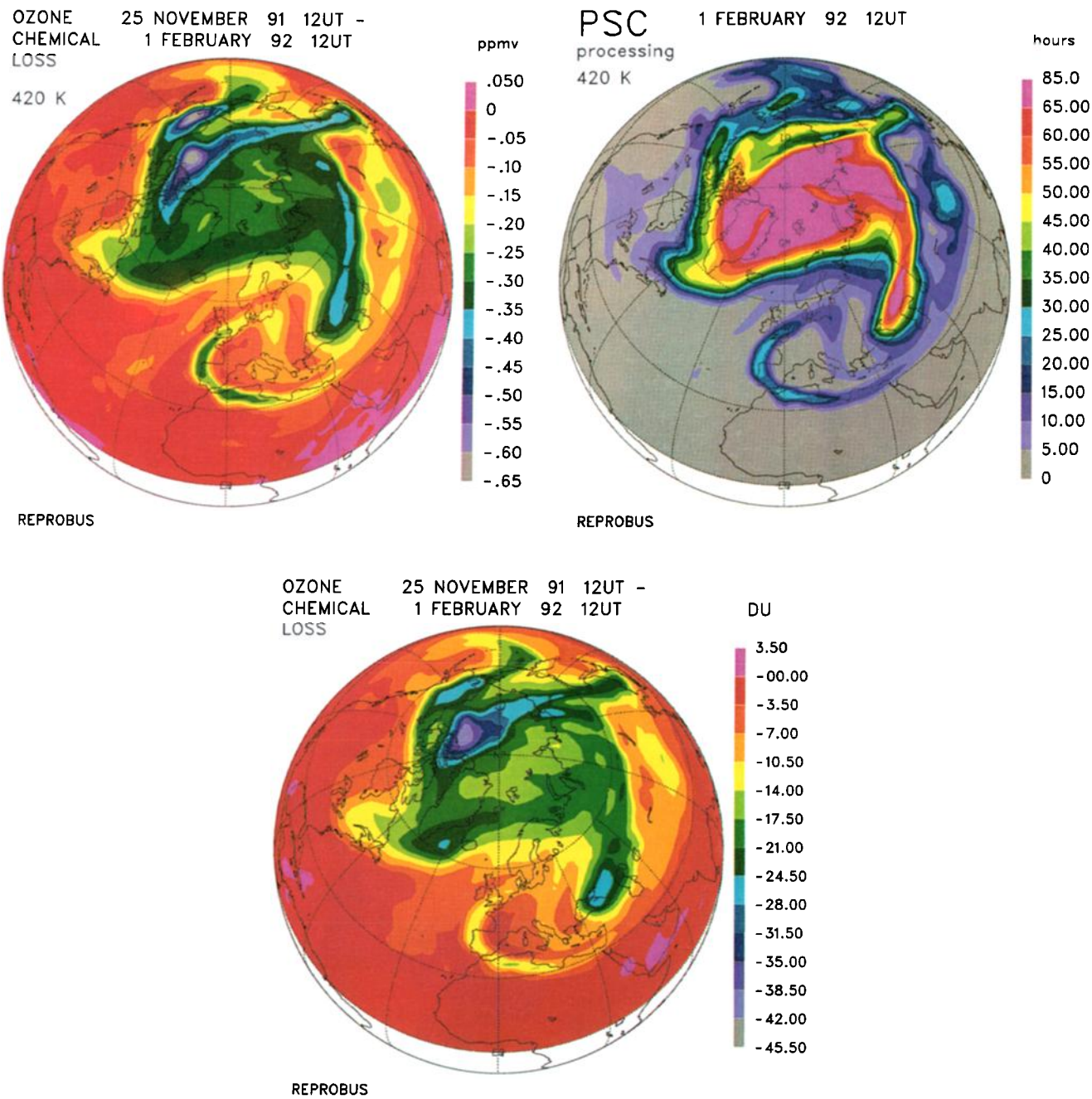

Plate 5. (a) Difference, in part per million by volume (ppmv) found at the end of the simulation (February 1, 1992) between the ozone mixing ratio calculated at 420 K when heterogeneous chemistry (PSC and aerosols) is taken into account and when it is ignored, (b) air processed by polar stratospheric clouds at 420 K at the end of the simulation, and (c) same as Plate 5a for the ozone column, in Dobson units.

stance, Plate 1a). As a result, on January 11 the maximum ozone depletion due to heterogeneous chemistry was approximately 10% at 50 hPa in the outer vortex. Under the influence of a strong minor warming in the upper stratosphere the stratospheric circulation became more perturbed during the second half of January, and the impact of heterogeneous chemistry progressively spread throughout the vortex. As the temperatures rose and large-scale PSCs disappeared after January 21, ClO and BrO abundances gradually decreased and the instantaneous destruction rate of ozone was reduced. The perturbation in ozone found at the end of the simulation on February 1, 1992, was estimated by comparing the concentrations of ozone determined when heterogeneous chemistry (PSCs and sulfate aerosol) is taken into account and when it is ignored. Because the "gas phase" and "heterogeneous" runs use the same dynamics without feedback with the chemistry, any difference in the ozone fields strictly results from photochemical loss (or production) due to

heterogeneous chemistry. At 420 K (about 16 km) our analysis reveals the greatest ozone loss expected in the outer part of the vortex, characterized both by elevated reactive chlorine and longer solar exposure (Plate 5*a*). The amount of ozone chemically destroyed in this region is between 0.3 and 0.5 ppmv (i.e., a 20-30% loss). Interestingly, the model also indicates losses of up to 0.3 ppmv confined inside blobs or filaments of air present at almost all longitudes at the periphery of the main vortex. From Plate 5*b* it may be seen that these ozone-depleted air parcels all coincide with peeled-off vortex material that experienced heterogeneous chemistry earlier in the simulation. This is consistent with the relatively free latitudinal exchange identified from ER-2 measurements at the bottom of the 1991-1992 Arctic vortex [*Proffitt et al.*, 1993] and illustrates again the potential significance of vortex erosion as an important contributor to midlatitude ozone loss. However, this process cannot explain the 30-50 ppbv reduction (5%) observed almost everywhere outside PSC-processed areas, which is therefore the result of heterogeneous chemistry on Pinatubo aerosols over the model integration period. The combined effects of PSC processing in the vortex, vortex erosion at low theta levels, and aerosols everywhere in midlatitude air led to substantial column ozone reductions in the model (Plate 5*c*), reaching more than 25 DU in the outer vortex. Nevertheless, the 10-20 DU chemical loss calculated over the North Atlantic and Scandinavia represents only a minor fraction of the total ozone deficit observed in January 1992, implying that chemical effects were largely outweighted by the dynamical effects associated with the presence of the strong blocking anticyclone in the troposphere over the Atlantic Ocean [*Naujokat et al.*, 1992].

Acknowledgments. We thank Joe Waters for supplying first results from MLS and for helpful discussions. Comments on this manuscript by Michael Coffey, Rolando Garcia, Steve Massie, and Darin Toohey are gratefully acknowledged. Franck Lefèvre was sponsored for this study by the Centre National d'Etudes Spatiales (CNES). Ian Folkins was partially supported by a National Sciences and Engineering Research Council of Canada (NSFRC) fellowship. The National Center for Atmospheric Research is funded by the National Science Foundation.

References

Abbatt, J. P. D., and M. J. Molina, The heterogeneous reaction of HOCl + HCl $\longrightarrow$ Cl_2 + H_2O on ice and nitric acid trihydrate: Reaction probabilities and stratospheric implications, *Geophys. Res. Lett., 19*, 461-464, 1992.

Brasseur, G. P., and C. Granier, Mount Pinatubo aerosols, chlorofluorocarbons, and ozone depletion, *Science, 257*, 1239-1242, 1992.

Brasseur, G. P., M. H. Hitchman, S. Walters, M. Dymek, E. Falise, and M. Pirre, An interactive chemical dynamical radiative two-dimensional model of the middle atmosphere, *J. Geophys. Res., 95*, 5639-5655, 1990.

Brune, W. H., J. G. Anderson, D. W. Toohey, D. W. Fahey, S. R. Kawa, R. L. Jones, D. S. McKenna, and L. R. Poole, The potential for ozone depletion in the arctic polar stratosphere, *Science, 252*, 1260-1266, 1991.

Burkholder, J. B., Ultraviolet absorption spectrum of HOCl, *J. Geophys. Res., 98*, 2963-2974, 1993.

Burkholder, J. B., R. K. Talukdar, A. R. Ravishankara, and S. Solomon, Temperature dependence of the HNO_3 UV absorption cross sections, *J. Geophys. Res., 98*, 22,937-22,948, 1993.

Chipperfield, M. P., D. Cariolle, P. Simon, R. Ramaroson, and D.J. Lary, A three-dimensional modeling study of trace species in the Arctic lower stratosphere during winter 1989-1990, *J. Geophys. Res., 98*, 7199-7218, 1993.

Crutzen, P. J., R. Mueller, C. Bruehl, and T. Peter, On the potential importance of the gas-phase reaction CH_3O_2 + ClO $\longrightarrow$ ClOO + CH_3O and the heterogeneous reaction HOCl + HCl $\longrightarrow$ H_2O + Cl_2 in ozone hole chemistry, *Geophys. Res. Lett., 19*, 1113-1116, 1992.

DeMore, W. B., et al.,Chemical kinetics and photochemical data for use in stratospheric modelling: Evaluation number 10, *Tech.Rep. 92-20*, Jet Propul. Lab., Pasadena, Calif. 1992.

Douglass, A., R. Rood, J. Waters, L. Froidevaux, W. Read, L. Elson, M. Geller, Y. Chi, M. Cerniglia, and S. Steenrood, A 3D simulation of the early winter distribution of reactive chlorine in the north polar vortex, *Geophys. Res. Lett., 20*, 1271-1274, 1993.

Fried, A., B. E. Henry, J. G. Calvert, and M. Mozurkewich, The reaction probability of N_2O_5 with sulfuric acid aerosols at stratospheric temperatures and compositions, *J. Geophys. Res., 99*, 3517-3532, 1994.

Hanson, D., and K. Mauersberger, Laboratory studies of the nitric acid trihydrate: Implications for the south polar stratosphere, *Geophys. Res. Lett., 15*, 855-858, 1988.

Hanson, D. R., and A. R. Ravishankara, The reaction probabilities of $ClONO_2$ and N_2O_5 on polar stratospheric cloud materials, *J. Geophys. Res., 96*, 5081-5090, 1991a.

Hanson, D. R., and A. R. Ravishankara, The reaction probabilities of $ClONO_2$ and N_2O_5 on 40 to 75% sulfuric acid solutions, *J. Geophys. Res., 96*, 17,307-17,314, 1991b.

Lefèvre, F., L. P. Riishojgaard, D. Cariolle, and P. Simon, Modeling the February 1990 polar stratospheric cloud event and its potential impact on the northern hemisphere ozone content, *J. Geophys. Res., 96*, 22,509- 22,534, 1991.

Molina, M. J., T. L. Tso, L. T. Molina, and F. C. Y. Wang, Antarctic stratospheric chemistry of chlorine nitrate, hydrogen chloride, and ice: Release of active chlorine, *Science, 238*, 1253-1257, 1987.

Mozurkewich, M., and J. G. Calvert, Reaction probability of N_2O_5 on aqueous aerosols, *J. Geophys. Res., 93*, 15889-15896, 1988.

Murphy, D. M., Ozone loss rates calculated along ER-2 flight tracks, *J. Geophys. Res., 96*, 5045-5053, 1991.

Murray, F. W., On the computation of saturation vapour pressure, *J. Appl. Meterol., 6*, 203-204, 1967.

National Aeronautics and Space Administration (NASA), Airborne Arctic Stratospheric Expedition II, *CD-ROM NASA/UARP- 004*, ed. 2, edited by S. Gaines, P. Hataway, and S. Hipskind, Ames Research Center, 1993.

Naujokat, B., K. Petzoldt, K. Labitzke, R. Lenschow, B. Rajewski, M. Wiesner, and R. C. Wohlfart, The stratospheric winter 1991/92: The winter of the European

Arctic Stratospheric Ozone Experiment, *Beil. Berl. Wetterkarte, 68/92*, Berlin, 1992.

Newman, P., L. R. Lait, M. Shoeberl, E. R. Nash, K. Kelly, D. W. Fahey, R. Nagatani, D. Toohey, L. Avallone, and J. Anderson, Stratospheric meteorological conditions in the Arctic polar vortex, 1991 to 1992, *Science, 261*, 1143-1146, 1993.

Proffitt, M. H., K. Aikin, J. J. Margitan, M. Loewenstein, J. R. Podolske, A. Weaver, K.R. Chan, H. Fast, and J.W. Elkins, Ozone loss inside the northern polar vortex during the 1991-1992 winter, *Science, 261*, 1150-1154, 1993.

Rosen, J. M., N. T. Kjome, and H. Fast, Penetration of Mt. Pinatubo aerosols into the north polar vortex, *Geophys. Res. Lett., 19*, 1751-1754, 1992.

Tolbert, M. A., M. J. Rossi, and D. M. Golden, Antarctic ozone depletion chemistry: Reactions of N_2O_5 with H_2O and HCl on ice surfaces, *Science, 240*, 1018-1021, 1988.

Toohey, D. W., L. M. Avallone, L. R. Lait, P. A. Newman, M. R. Schoeberl, D. W. Fahey, E. L. Woodbridge, and J. G. Anderson, The seasonal evolution of reactive chlorine in the northern hemisphere stratosphere, *Science, 261*, 1134-1136, 1993.

Tuck, A. F., et al., Polar stratospheric cloud processed air and potential vorticity in the northern hemisphere lower stratosphere at midlatitudes during winter, *J. Geophys. Res., 97*, 7883-7904, 1992.

Waters, J. W., L. Froidevaux, W. G. Read , G. L. Manney, L. S. Elson, D. A. Flower, R. F. Jarnot, and R. S. Harwood, Stratospheric ClO and ozone from the Microwave Limb Sounder on the Upper Atmosphere Research Satellite, *Nature, 362*, 597-602, 1993.

Webster, C. R., R. D. May, D. W. Toohey, L. M. Avallone, J. G. Anderson, P. Newman, L. Lait, M. R. Schoeberl, J. W. Elkins, and K. R. Chan, Chlorine chemistry on polar stratospheric cloud particles in the Arctic winter, *Science, 261*, 1130-1134, 1993.

Williamson, D. L., and P.J. Rasch, Two-dimensional semi-lagrangian transport with shape-preserving interpolation, *Mon. Weather Rev., 117*, 102-129, 1989.

World Meteorological Organization, (WMO), Ozone data for the world, Downsview, Ontario, 1992a.

World Meteorological Organization, (WMO),Scientific assessment of ozone depletion: 1991, in *Global Ozone Research and Monitoring Project, WMO Rep. 25*, Geneva, 1992b.

G. P. Brasseur and A. K. Smith, National Center for Atmospheric Research, P.O. Box 3000, Boulder, CO 80307.

I. Folkins, Department of Oceanography, Dalhousie University, Halifax, Nova Scotia, Canada B3H 3J5.

F. Lefèvre and P. Simon, Météo-France, Centre National de Recherches Météorologiques, 31057 Toulouse Cedex, France. E-mail: franck.lefevre@meteo.fr.

(Received July 22, 1993; revised December 5, 1993; accepted December 5, 1993.)